

SIMPLE CURL-CURL-CONFORMING FINITE ELEMENTS IN TWO DIMENSIONS*

KAIBO HU[†], QIAN ZHANG[‡], AND ZHIMIN ZHANG[§]

Abstract. We construct smooth finite element de Rham complexes in two space dimensions. This leads to three families of curl-curl-conforming finite elements, two of which contain two existing families. The simplest triangular and rectangular finite elements have only six and eight degrees of freedom, respectively. Numerical experiments for each family demonstrate the convergence and efficiency of the elements for solving the quad-curl problem.

Key words. $H(\text{curl}^2)$ -conforming, finite elements, de Rham complexes, exterior calculus, quad-curl problems

AMS subject classifications. 65N30, 35Q60, 65N15, 35B45

DOI. 10.1137/20M1333390

1. Introduction. In this paper, we construct and analyze three families of curl-curl-conforming ($H(\text{curl}^2)$ -conforming) finite elements in two space dimensions (2D) and use these elements to solve the quad-curl problem.

The quad-curl equation appears in various models, such as inverse electromagnetic scattering theory [8, 15, 18] and magnetohydrodynamics [26]. The corresponding quad-curl eigenvalue problem plays a fundamental role in the analysis and computation of the electromagnetic interior transmission eigenvalues [17]. Some methods have been developed for the source problem and the eigenvalue problem in, e.g., [6, 7, 9, 14, 18, 19, 20, 21, 22, 23, 24, 25, 26]. Recently, two of the authors and a collaborator together developed for the first time a family of curl-curl-conforming finite elements [23]. To reduce the number of degrees of freedom (DOFs), they used incomplete polynomials. The polynomial degree k starts from four for triangular elements and three for rectangular elements, respectively, and the lowest-order elements of both shapes have 24 DOFs. Moreover, in [22] they collaborated with Sun and constructed another family of curl-curl-conforming triangular elements with complete polynomials. The polynomial degree k starts from four, and hence the lowest-order element has 30 DOFs. In this paper, in addition to the construction of new $H(\text{curl}^2)$ -conforming elements, we fit the two existing families into complexes and extend them to lower-order cases.

The discrete de Rham complex is now an important tool for the construction of finite elements and the analysis of numerical schemes; cf. [1, 3, 4, 10, 13, 16]. In this direction, the finite element periodic table [5] includes various successful finite elements for computational electromagnetism or diffusion problems. Motivated by

*Submitted to the journal's Methods and Algorithms for Scientific Computing section April 23, 2020; accepted for publication (in revised form) September 17, 2020; published electronically December 14, 2020.

<https://doi.org/10.1137/20M1333390>

Funding: This work was partially supported by the National Natural Science Foundation of China through grants NSFC 11871092 and NSAF U1930402.

[†]School of Mathematics, University of Minnesota, Minneapolis, MN 55455 USA (khu@umn.edu).

[‡]Corresponding author. Department of Mathematics, Wayne State University, Detroit, MI 48202 USA (go9563@wayne.edu).

[§]Beijing Computational Science Research Center, Beijing 100193, China (zmzhang@csrc.ac.cn), and Department of Mathematics, Wayne State University, Detroit, MI 48202 USA (ag7761@wayne.edu).

problems in fluid and solid mechanics, researchers have taken an increased interest in constructing finite element de Rham complexes with enhanced smoothness, sometimes referred to as Stokes complexes [11, 12]. In this paper, for the discretization of the quad-curl problem, we will consider another variant of the de Rham complex, i.e.,

$$(1.1) \quad 0 \longrightarrow \mathbb{R} \xrightarrow{\subset} H^1(\Omega) \xrightarrow{\nabla} H(\text{curl}^2; \Omega) \xrightarrow{\nabla \times} H^1(\Omega) \longrightarrow 0,$$

where Ω is a bounded Lipschitz domain in \mathbb{R}^2 , and

$$H(\text{curl}^2; \Omega) := \{\mathbf{u} \in \mathbf{L}^2(\Omega) : \nabla \times \mathbf{u} \in L^2(\Omega), \nabla \times \nabla \times \mathbf{u} \in \mathbf{L}^2(\Omega)\}.$$

For simplicity of the presentation, throughout this paper we will assume that Ω is contractible. Then the exactness of (1.1) follows from standard results in, e.g., [1].

This complex point of view makes it possible to achieve the goal of this paper, i.e., constructing simple curl-curl-conforming elements with fewer DOFs, compared to, e.g., those in [23] and [22]. From this complex perspective, we also fit the quad-curl problem and its finite element approximations into the framework of finite element exterior calculus (FEEC) [1, 3]. Thus, a number of tools from FEEC can be used for the numerical analysis. For example, we construct interpolation operators that commute with the differential operators. Then the convergence result follows from a standard argument.

Specifically, the new finite elements fit into a subcomplex of (1.1):

$$(1.2) \quad 0 \longrightarrow \mathbb{R} \xrightarrow{\subset} \Sigma_h \xrightarrow{\nabla} V_h \xrightarrow{\nabla \times} W_h \longrightarrow 0.$$

In (1.2), we choose Lagrange finite element spaces for Σ_h and Lagrange elements enriched with bubbles for W_h . The space $V_h \subset H(\text{curl}^2; \Omega)$ is thus obtained as the gradient of Σ_h plus a complementary part, which is mapped onto W_h by curl. We will use V_h as a conforming finite element for solving the quad-curl problem below. Among the three versions of V_h which we will construct in this paper, the simplest elements have only six DOFs for a triangle and eight DOFs for a rectangle. To the best of our knowledge, these elements have the smallest number of DOFs among all the existing curl-curl-conforming finite elements.

The significance of this new development is threefold: (1) It develops new families of curl-curl-conforming elements; (2) it relates the curl-curl-conforming elements to the FEEC via the de Rham complex, thereby allowing further systematic development of new elements; and (3) it reduces element DOFs of the existing lowest-order curl-curl-conforming element from 24 to six and eight for triangular and rectangular elements, respectively, which makes commercial adoption of the elements feasible.

The remainder of the paper is organized as follows. In section 2, we present notation and preliminaries. In section 3, we define shape functions and local exact sequences by the Poincaré operators and prove their properties. In section 4, we construct a new family of curl-curl-conforming finite elements. Then in section 5 we extend two existing families to lower-order cases by fitting them into complexes. In section 6, we provide numerical examples to verify the correctness and efficiency of our method. Concluding remarks and future work are given in section 7. In the appendix, we list the basis functions of the lowest-order elements in the new family.

2. Preliminaries. Let $\Omega \in \mathbb{R}^2$ be a contractible Lipschitz domain. We adopt standard notation for Sobolev spaces such as $H^m(D)$ or $H_0^m(D)$ on a simply connected subdomain $D \subset \Omega$ equipped with the norm $\|\cdot\|_{m,D}$ and the seminorm $|\cdot|_{m,D}$. If

$m = 0$, the space $H^0(D)$ coincides with $L^2(D)$ equipped with the norm $\|\cdot\|_D$, and when $D = \Omega$, we drop the subscript D . We use $\mathbf{H}^m(D)$ and $\mathbf{L}^2(D)$ to denote the vector-valued Sobolev spaces $[H^m(D)]^2$ and $[L^2(D)]^2$.

Let $\mathbf{u} = (u_1, u_2)^T$ and $\mathbf{w} = (w_1, w_2)^T$, where the superscript T denotes the transpose. Then $\mathbf{u} \times \mathbf{w} = u_1 w_2 - u_2 w_1$ and $\nabla \times \mathbf{u} = \partial_{x_1} u_2 - \partial_{x_2} u_1$. For a scalar function v , $\nabla \times v = (\partial_{x_2} v, -\partial_{x_1} v)^T$. We denote $(\nabla \times)^2 \mathbf{u} = \nabla \times \nabla \times \mathbf{u}$.

We define

$$\begin{aligned} H(\text{curl}; D) &:= \{\mathbf{u} \in \mathbf{L}^2(D) : \nabla \times \mathbf{u} \in L^2(D)\}, \\ H(\text{curl}^2; D) &:= \{\mathbf{u} \in \mathbf{L}^2(D) : \nabla \times \mathbf{u} \in L^2(D), \nabla \times \nabla \times \mathbf{u} \in \mathbf{L}^2(D)\}, \end{aligned}$$

with the scalar product and norm

$$(\mathbf{u}, \mathbf{v})_{H(\text{curl}^s; D)} = (\mathbf{u}, \mathbf{v}) + \sum_{j=1}^s ((\nabla \times)^j \mathbf{u}, (\nabla \times)^j \mathbf{v}),$$

and

$$\|\mathbf{u}\|_{H(\text{curl}^s; D)} = \sqrt{(\mathbf{u}, \mathbf{u})_{H(\text{curl}^s; D)}},$$

with $s = 1, 2$.

We use $Q_{i,j}(D)$ to denote the polynomials with two variables (x_1, x_2) where the maximal degree is i in x_1 and j in x_2 . For simplicity, we drop the subscript i when $i = j$. We use $P_i(D)$ to represent the space of polynomials on D with a degree no larger than i and $\mathbf{P}_i(D) = [P_i(D)]^2$. We denote by $\tilde{P}_i(D)$ the space of homogeneous polynomials.

Let \mathcal{T}_h be a partition of the domain Ω consisting of shape regular rectangles or triangles. We denote by h_K the diameter of an element $K \in \mathcal{T}_h$ and by h the mesh size of \mathcal{T}_h . We use C to denote a generic positive h -independent constant.

Let $\mathfrak{p} : C^\infty(\mathbb{R}^2) \mapsto [C^\infty(\mathbb{R}^2)]^2$ be an operator which maps a scalar function to a vector field:

$$\mathfrak{p}u := \int_0^1 t \mathbf{x}^\perp u(t \mathbf{x}) dt,$$

where

$$\mathbf{x} := (x_1, x_2)^T \quad \text{and} \quad \mathbf{x}^\perp := (-x_2, x_1)^T.$$

As a special case of the Poincaré operators (cf. [11, 13]), \mathfrak{p} has the following properties:

- polynomial preserving property: if $u \in P_r(\mathbb{R}^2)$, then $\mathfrak{p}u \in \mathbf{P}_{r+1}(\mathbb{R}^2)$;
- the null-homotopy identity

$$(2.1) \quad \nabla \times \mathfrak{p}u = u, \quad \forall u \in C^\infty(\mathbb{R}^2).$$

We review some basic facts from homological algebra; further details can be found, for instance, in [3]. A differential complex is a sequence of spaces V^i and operators d^i such that

$$(2.2) \quad 0 \longrightarrow V^1 \xrightarrow{d^1} V^2 \xrightarrow{d^2} \cdots \xrightarrow{d^{n-1}} V^n \xrightarrow{d^n} 0,$$

satisfying the complex property $d^{i+1} d^i = 0$ for $i = 1, 2, \dots, n-1$. Let $\ker(d^i)$ be the kernel space of the operator d^i in V^i , and let $\text{ran}(d^i)$ be the image of the operator d^i in V^{i+1} . Due to the complex property, we have $\ker(d^i) \subset \text{ran}(d^{i-1})$ for each $i \geq 2$.

Furthermore, if $\ker(d^i) = \text{ran}(d^{i-1})$, we say that the complex (2.2) is exact at V^i . At the two ends of the sequence, the complex is exact at V^1 if d^1 is injective (with trivial kernel) and is exact at V^n if d^{n-1} is surjective (with trivial cokernel). The complex (2.2) is called exact if it is exact at all the spaces V^i . If each space in (2.2) has finite dimensions, then a necessary (but not sufficient) condition for the exactness of (2.2) is the following dimension condition:

$$\sum_{i=1}^n (-1)^i \dim(V^i) = 0.$$

3. Local spaces and polynomial complexes. To define a finite element space, for each element $K \in \mathcal{T}_h$ we must supply the space of shape functions and the DOFs. We will use the following complexes as the local function spaces on each $K \in \mathcal{T}_h$ for (1.2):

$$(3.1) \quad 0 \longrightarrow \mathbb{R} \xrightarrow{\subseteq} \Sigma_h^r(K) \xrightarrow{\nabla} V_h^{r-1,k}(K) \xrightarrow{\nabla \times} W_h^{k-1}(K) \longrightarrow 0.$$

Let $\Sigma_h^r(K)$ be $P_r(K)$ for a triangular element or $Q_r(K)$ for a rectangular element. For a triangular element K , we set

$$W_h^{k-1}(K) = \begin{cases} P_{k-1}(K), & k \geq 4, \\ P_{k-1}(K) \oplus \text{span}\{B_t\}, & k = 2, 3, \end{cases}$$

where $B_t = \lambda_1 \lambda_2 \lambda_3$ with the barycentric coordinate λ_i . For a rectangular element K , we set

$$W_h^{k-1}(K) = \begin{cases} Q_{k-1}(K), & k \geq 3, \\ Q_{k-1}(K) \oplus \text{span}\{B_r\}, & k = 2, \end{cases}$$

where $B_r = h_x^{-2} h_y^{-2} (x - x_l)(x - x_r)(y - y_d)(y - y_u)$ with the element $K = (x_l, x_r) \times (y_d, y_u)$ and $h_x = x_r - x_l$, $h_y = y_u - y_d$. We define

$$(3.2) \quad V_h^{r-1,k}(K) = \nabla \Sigma_h^r(K) \oplus \mathfrak{p}W_h^{k-1}(K).$$

Remark 3.1. For a rectangular element, we can also use the serendipity elements $S_r(K) = P_r(K) \oplus \text{span}\{x_1^r x_2, x_1 x_2^r\}$ [2] for $\Sigma_h^r(K)$ and use $S_{k-1}(K)$ when $k \geq 5$ ($S_{k-1}(K) \oplus \text{span}\{B_r\}$ when $k < 5$) for W_h^{k-1} . This leads to another three families of rectangular elements with fewer DOFs and the same accuracy.

Remark 3.2. The Koszul operator $\kappa u := ux^\perp$ has properties similar to those of the Poincaré operator [1, 3]. Therefore, for polynomial bases in $W_h^{k-1}(K)$ other than the bubble B_t or B_r , we can replace the Poincaré operator by the Koszul operator. For the bubble function B_t on the reference triangle with vertices $(0, 0)$, $(0, 1)$, and $(1, 0)$, or for B_r on the reference rectangle $(-1, 1) \times (-1, 1)$, we have, respectively,

$$\begin{aligned} \mathfrak{p}B_t &= \frac{x_1 x_2 (4x_1 + 4x_2 - 5)}{20} x^\perp, \\ \mathfrak{p}B_r &= \frac{2x_1^2 x_2^2 - 3x_1^2 - 3x_2^2 + 6}{12} x^\perp. \end{aligned}$$

By the null-homotopy identity (2.1), the right-hand side of (3.2) is a direct sum.

LEMMA 3.3. *The local sequence (3.1) is a complex and exact.*

Proof. Since $V_h^{r-1,k}(K) = \nabla \Sigma_h^r(K) + \mathfrak{p}W_h^{k-1}(K)$ and the null-homotopy identity (2.1) holds, we have $\nabla \Sigma_h^r(K) \subseteq V_h^{r-1,k}(K)$ and $\nabla \times V_h^{r-1,k}(K) = W_h^{k-1}(K)$. This shows that (3.1) is a complex. It remains to show the exactness. We first show that, for any $\mathbf{v}_h \in V_h^{r-1,k}(K)$ for which $\nabla \times \mathbf{v}_h = 0$, there exists a $p_h \in \Sigma_h^r(K)$ such that $\mathbf{v}_h = \nabla p_h$. Since $\mathbf{v}_h \in V_h^{r-1,k}$, we have $\mathbf{v}_h = \nabla p_h + \mathfrak{p}w_h$ with $p_h \in \Sigma_h^r(K)$ and $w_h \in W_h^{k-1}(K)$. By the null-homotopy identity (2.1) again, $0 = \nabla \times \mathbf{v}_h = w_h$. Therefore, $\mathbf{v}_h = \nabla p_h$. Moreover, the curl operator $\nabla \times : V_h^{r-1,k}(K) \rightarrow W_h^{k-1}(K)$ is surjective since $\nabla \times V_h^{r-1,k}(K) = W_h^{k-1}(K)$. \square

In the following lemma, we show that $V_h(K)^{r-1,k}$ contains some polynomial subspaces.

LEMMA 3.4. *Suppose that $r \leq k+1$. Then $\mathbf{P}_{r-1}(K) \subseteq V_h^{r-1,k}(K)$.*

Proof. We claim that

$$(3.3) \quad \mathbf{P}_{r-1}(K) = \nabla P_r(K) \oplus \mathfrak{p}P_{r-2}(K).$$

In fact, $\nabla P_r(K) \oplus \mathfrak{p}P_{r-2}(K) \subseteq \mathbf{P}_{r-1}(K)$. To show (3.3), we only need to show

$$\dim \nabla P_r(K) \oplus \mathfrak{p}P_{r-2}(K) = \dim \mathbf{P}_{r-1}(K).$$

By the null-homotopy identity (2.1), the right-hand side is a direct sum. Therefore,

$$(3.4) \quad \begin{aligned} \dim \nabla P_r(K) \oplus \mathfrak{p}P_{r-2}(K) &= \dim \nabla P_r(K) + \dim P_{r-2}(K) \\ &= \frac{(r+1)(r+2)}{2} + \frac{(r-1)r}{2} - 1 = r(r+1), \end{aligned}$$

which is exactly the dimension of $\mathbf{P}_{r-1}(K)$.

Combining (3.3) and the facts that $P_{r-2}(K) \subseteq W_h^{k-1}(K)$ and $P_r(K) \subseteq \Sigma_h^r(K)$, we get $\mathbf{P}_{r-1}(K) \subseteq \nabla \Sigma_h^r(K) \oplus \mathfrak{p}W_h^{k-1}(K) = V_h^{r-1,k}(K)$. \square

In the following sections, we will take different values of r to get various families of curl-curl-conforming finite elements and complexes. In section 4, we take $r = k-1$, and this leads to a new family of simple elements. In section 5, we introduce the other two families of elements by taking $r = k, k+1$, respectively.

4. A new family of curl-curl-conforming elements $r = k-1$. In this section, we construct a new family of curl-curl-conforming elements $V_h^{k-2,k}$ by specifying $r = k-1$ in (3.1), i.e.,

$$(4.1) \quad 0 \longrightarrow \mathbb{R} \xrightarrow{\subset} \Sigma_h^{k-1} \xrightarrow{\nabla} V_h^{k-2,k} \xrightarrow{\nabla \times} W_h^{k-1} \longrightarrow 0.$$

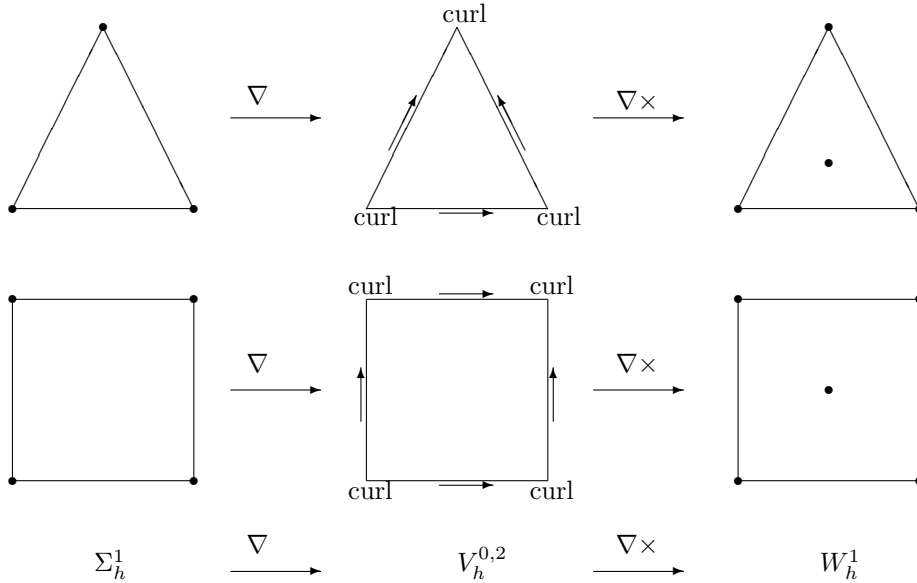
For simplicity of the presentation, we focus on the triangular elements and mention only the rectangular elements in Remark 4.8 below. The sequence of the lowest-order case is shown in Figure 1.

4.1. Degrees of freedom and global finite element spaces. We define DOFs for the spaces in (4.1).

The DOFs for the Lagrange element Σ_h^r can be given as follows:

- Vertex DOFs $M_v(u)$ at all the vertices v_i of K :

$$M_v(u) = \{u(v_i), i = 1, 2, 3, 4\}.$$

FIG. 1. The lowest-order ($k = 2$) finite element complex (4.1) in 2D.

- Edge DOFs $M_e(u)$ on all the edges e_i of K :

$$M_e(u) = \left\{ \int_{e_i} uv ds \quad \forall v \in P_{r-2}(e_i), \quad i = 1, 2, 3, 4 \right\}.$$

- Interior DOFs $M_K(u)$:

$$M_K(u) = \left\{ \int_K uv dA \quad \forall v \in P_{r-3}(K) \text{ or } Q_{r-2}(K) \right\}.$$

For $u \in H^{1+\delta}(\Omega)$ with $\delta > 0$, we can define an H^1 interpolation operator π_h by the above DOFs. The restriction of π_h on K is denoted as π_K and defined by

$$(4.2) \quad M_v(u - \pi_K u) = \{0\}, \quad M_e(u - \pi_K u) = \{0\}, \quad \text{and} \quad M_K(u - \pi_K u) = \{0\}.$$

The DOFs for W_h^{k-1} can be given similarly, with only one additional interior integration DOF on K to take care of the interior bubble. We denote by $\tilde{\pi}_h$ the H^1 interpolation operator to W_h^{k-1} by these DOFs.

For the shape function space $V_h^{k-2,k}(K) := \nabla P_{k-1}(K) \oplus \mathfrak{p}W_h^{k-1}(K)$ of the triangular elements, we define the following DOFs:

- Vertex DOFs $\mathbf{M}_v(\mathbf{u})$ at all the vertices v_i of K :

$$(4.3) \quad \mathbf{M}_v(\mathbf{u}) = \{(\nabla \times \mathbf{u})(v_i), \quad i = 1, 2, 3\}.$$

- Edge DOFs $\mathbf{M}_e(\mathbf{u})$ at all the edges e_i of K (with the unit tangential vector $\boldsymbol{\tau}_i$):

$$(4.4) \quad \begin{aligned} \mathbf{M}_e(\mathbf{u}) = & \left\{ \int_{e_i} \mathbf{u} \cdot \boldsymbol{\tau}_i q ds \quad \forall q \in P_{k-2}(e_i), \quad i = 1, 2, 3 \right\} \\ & \cup \left\{ \int_{e_i} \nabla \times \mathbf{u} q ds \quad \forall q \in P_{k-3}(e_i), \quad i = 1, 2, 3 \right\}. \end{aligned}$$

- Interior DOFs $\mathbf{M}_K(\mathbf{u})$:

$$(4.5) \quad \mathbf{M}_K(\mathbf{u}) = \left\{ \int_K \mathbf{u} \cdot \mathbf{q} dA \mid \mathbf{q} \in \mathcal{D} \right\},$$

where $\mathcal{D} = \mathbf{P}_{k-5}(K) \oplus \tilde{\mathbf{P}}_{k-5}\mathbf{x} \oplus \tilde{\mathbf{P}}_{k-4}\mathbf{x}$ with $\mathbf{x} = (x_1, x_2)^T$ when $k \geq 5$, $\mathcal{D} = P_0\mathbf{x}$ when $k = 4$, and $\mathcal{D} = \emptyset$ when $k = 2, 3$.

LEMMA 4.1. *The DOFs (4.3)–(4.5) are well defined for any $\mathbf{u} \in \mathbf{H}^{1/2+\delta}(K)$ and $\nabla \times \mathbf{u} \in H^{1+\delta}(K)$ with $\delta > 0$.*

The proof of this lemma is the same as that of Lemma 3.4 in [23]. We omit it here.

LEMMA 4.2. *The DOFs for $V_h^{k-2,k}(K)$ are unisolvant.*

Proof. The decomposition (3.2) is a direct sum. Therefore, $\dim V_h^{k-2,k}(K) = \dim \nabla \Sigma_h^{k-1}(K) + \dim W_h^{k-1}(K) = k(k+1) - 1$ when $k \geq 4$, and $\dim V_h^{k-2,k}(K) = k(k+1)$ when $k = 2, 3$. By counting the number of DOFs, we see that they have the same dimension. Then it suffices to show that if all the DOFs vanish on a function \mathbf{u} , then $\mathbf{u} = 0$. To see this, we first observe that $\nabla \times \mathbf{u} = 0$ by the unisolvence of the DOFs of $W_h^{k-1}(K)$. Then $\mathbf{u} = \nabla \phi \in P_{k-2}(K)$ for some $\phi \in \Sigma_h^{k-1}(K)$. By the edge DOFs of $V_h^{k-2,k}(K)$, $\mathbf{u} \cdot \boldsymbol{\tau} = 0$ on edges. Then there exists some $\psi \in P_{k-4}(K)$ such that $\phi = \lambda_1 \lambda_2 \lambda_3 \psi$. Choosing $\mathbf{q} \in P_{k-4}(K)\mathbf{x}$ for which $\nabla \cdot \mathbf{q} = \psi$, we have by the interior DOFs

$$0 = (\mathbf{u}, \mathbf{q}) = (\nabla \phi, \mathbf{q}) = -(\phi, \nabla \cdot \mathbf{q}) = (\lambda_1 \lambda_2 \lambda_3 \psi, \psi).$$

This implies that $\psi = 0$ and hence that $\phi = 0$ and $\mathbf{u} = 0$. \square

Provided that $\mathbf{u} \in \mathbf{H}^{1/2+\delta}(\Omega)$ and that $\nabla \times \mathbf{u} \in H^{1+\delta}(\Omega)$ with $\delta > 0$ (see Lemma 4.1), we can define an $H(\text{curl}^2)$ interpolation operator Π_h whose restriction on K is denoted by Π_K and defined by

$$(4.6) \quad \mathbf{M}_v(\mathbf{u} - \Pi_K \mathbf{u}) = \{0\}, \quad \mathbf{M}_e(\mathbf{u} - \Pi_K \mathbf{u}) = \{0\}, \quad \text{and } \mathbf{M}_K(\mathbf{u} - \Pi_K \mathbf{u}) = \{0\},$$

where \mathbf{M}_v , \mathbf{M}_e , and \mathbf{M}_K are the sets of DOFs in (4.3)–(4.5).

Gluing the local spaces by the above DOFs, we obtain the global finite element spaces Σ_h^{k-1} , $V_h^{k-2,k}$, and W_h^{k-1} .

LEMMA 4.3. *The following conformity holds:*

$$V_h^{k-2,k} \subset H(\text{curl}^2; \Omega).$$

Proof. The proof is straightforward since $\nabla \times V_h^{k-2,k} \subseteq W_h^{k-1} \subset H^1(\Omega)$. \square

4.2. Global finite element complexes for the quad-curl problem. The global finite element spaces lead to a complex which is exact on contractible domains.

THEOREM 4.4. *The complex (4.1) is exact on contractible domains.*

Proof. We first show the exactness at $V_h^{k-2,k}$. To this end, we show that for any $\mathbf{v}_h \in V_h^{k-2,k} \subset H(\text{curl}^2; \Omega)$ satisfying $\nabla \times \mathbf{v}_h = 0$, there exists $p \in \Sigma_h^{k-1}$ such that $\mathbf{v}_h = \nabla p$. Actually, this follows from the exactness of the standard finite element differential forms (e.g., [1]) and the fact that the curl-free part of $V_h^{k-2,k}$ is a subspace of the second Nédélec space of degree $k - 2$. To prove the exactness at W_h^{k-1} , that

is, to prove that the operator $\nabla \times$ from $V_h^{k-2,k}$ to W_h^{k-1} is surjective, we count the dimensions. The dimension count of the Lagrange elements reads

$$\dim \Sigma_h^{k-1} = \mathcal{V} + (k-2)\mathcal{E} + \frac{1}{2}(k-3)(k-2)\mathcal{F},$$

where \mathcal{V} , \mathcal{E} , and \mathcal{F} denote the number of vertices, edges, and 2D cells, respectively. Moreover, $\dim W_h^{k-1} = \dim \Sigma_h^{k-1}$ for $k \geq 4$ and $\dim W_h^{k-1} = \dim \Sigma_h^{k-1} + \mathcal{F}$ for $k = 2, 3$. From the DOFs (4.3)–(4.5),

$$\begin{aligned}\dim V_h^{k-2,k} &= \mathcal{V} + (2k-3)\mathcal{E} + (k^2 - 5k + 5)\mathcal{F} \text{ for } k \geq 4, \\ \dim V_h^{k-2,k} &= \mathcal{V} + (2k-3)\mathcal{E} \text{ for } k = 2, 3.\end{aligned}$$

From the above dimension count, we have

$$\dim V_h^{k-2,k} = \dim W_h^{k-1} + \dim \Sigma_h^{k-1} - 1,$$

where we have used Euler's formula $\mathcal{V} - \mathcal{E} + \mathcal{F} = 1$. This completes the proof. \square

We summarize the interpolations defined in section 4.1 in the following diagram:

$$(4.7) \quad \begin{array}{ccccccc} 0 & \longrightarrow & \mathbb{R} & \xrightarrow{\subset} & H^1(\Omega) & \xrightarrow{\nabla} & H(\operatorname{curl}^2; \Omega) & \xrightarrow{\nabla \times} & H^1(\Omega) & \longrightarrow & 0 \\ & & & & \downarrow & & \downarrow & & \downarrow & & \\ 0 & \longrightarrow & \mathbb{R} & \xrightarrow{\subset} & W & \xrightarrow{\nabla} & V & \xrightarrow{\nabla \times} & W & \longrightarrow & 0 \\ & & & & \downarrow \pi_h & & \downarrow \Pi_h & & \downarrow \tilde{\pi}_h & & \\ 0 & \longrightarrow & \mathbb{R} & \xrightarrow{\subset} & \Sigma_h^{k-1} & \xrightarrow{\nabla} & V_h^{k-2,k} & \xrightarrow{\nabla \times} & W_h^{k-1} & \longrightarrow & 0, \end{array}$$

where W and V are two subspaces of $H^1(\Omega)$ and $H(\operatorname{curl}^2; \Omega)$ in which π_h (or $\tilde{\pi}_h$) and Π_h are well defined.

Now we show that the interpolations in (4.7) commute with the differential operators. This result will play a key role in the error analysis below for discretizing the quad-curl problem.

LEMMA 4.5. *The last two rows of the complex (4.7) are a commuting diagram, i.e.,*

$$(4.8) \quad \nabla \pi_h u = \Pi_h \nabla u \quad \forall u \in W,$$

$$(4.9) \quad \nabla \times \Pi_h \mathbf{u} = \tilde{\pi}_h \nabla \times \mathbf{u} \quad \forall \mathbf{u} \in V.$$

Proof. We only prove (4.8). A similar trick can be used to prove (4.9). From the diagram (4.7), we know both $\Pi_h \nabla u$ and $\nabla \pi_h u$ are in the space $V_h^{k-2,k}$. It suffices to prove that the DOFs (4.3)–(4.5) for $\Pi_h \nabla u$ and $\nabla \pi_h u$ agree element by element. For a given element K with a vertex v_i , we first have

$$\nabla \times (\Pi_h \nabla u - \nabla \pi_h u)(v_i) = \nabla \times (\nabla u - \nabla \pi_h u)(v_i) = 0.$$

On an edge e_i with a tangent vector τ_i and two vertices v_1 and v_2 , for any $q \in P_{k-2}(e_i)$, we derive

$$\begin{aligned}\int_{e_i} (\Pi_h \nabla u - \nabla \pi_h u) \cdot \tau_i q ds &= \int_{e_i} (\nabla u - \nabla \pi_h u) \cdot \tau_i q ds \\ &= p(v_2)(u - \pi_h u)(v_2) - p(v_1)(u - \pi_h u)(v_1) - \int_{e_i} (u - \pi_h u) \frac{\partial q}{\partial \tau_i} ds = 0.\end{aligned}$$

Here we used integration by parts and the definition of the interpolations. By the definition of Π_h , we have

$$\int_{e_i} \nabla \times (\Pi_h \nabla u - \nabla \pi_h u) q ds = 0.$$

For the interior DOFs, we see that for any $\mathbf{q} \in \mathbf{P}_{k-3}(K)$,

$$\begin{aligned} \int_K (\Pi_h \nabla u - \nabla \pi_h u) \cdot \mathbf{q} dS &= \int_K (\nabla u - \nabla \pi_h u) \cdot \mathbf{q} dS \\ &= - \int_K (u - \pi_h u) \nabla \cdot \mathbf{q} dS + \int_{\partial K} (u - \pi_h u) \mathbf{q} \cdot \mathbf{n} ds = 0. \end{aligned}$$

This completes the proof. \square

THEOREM 4.6. *If $\mathbf{u} \in \mathbf{H}^{s-1}(\Omega)$ and $\nabla \times \mathbf{u} \in H^s(\Omega)$, $1 + \delta \leq s \leq k$ with $\delta > 0$, then we have the following error estimates for the interpolation Π_h :*

$$(4.10) \quad \|\mathbf{u} - \Pi_h \mathbf{u}\| \leq Ch^{s-1} (\|\mathbf{u}\|_{s-1} + \|\nabla \times \mathbf{u}\|_s),$$

$$(4.11) \quad \|\nabla \times (\mathbf{u} - \Pi_h \mathbf{u})\| \leq Ch^s \|\nabla \times \mathbf{u}\|_s,$$

$$(4.12) \quad \|(\nabla \times)^2 (\mathbf{u} - \Pi_h \mathbf{u})\| \leq Ch^{s-1} \|\nabla \times \mathbf{u}\|_s.$$

Proof. From Lemma 3.4, $\mathbf{P}_{k-2}(K) \subseteq V_h^{k-2,k}(K)$ and $\mathbf{P}_{k-1}(K) \subseteq W_h^{k-1}(K)$. By a similar proof of Theorem 3.11 in [23] and using Lemma 4.5, we complete the proof. \square

Remark 4.7. Here, we only provide the approximation property for the interpolation $\Pi_h \mathbf{u}$. Since $V_h^{k-2,k}$ is a conforming finite element space, the approximation property of the numerical solution \mathbf{u}_h follows immediately from Céa's lemma. It is the same for the other two families.

Remark 4.8. Similarly, we can get a family of rectangular elements. The DOFs for $\mathbf{u} \in V_h^{k-2,k}(K) = \nabla Q_{k-1}(K) + \mathfrak{p}W_h^{k-1}(K)$ are given by the following:

- Vertex DOFs $\mathbf{M}_v(\mathbf{u})$ at all the vertices v_i of K :

$$\mathbf{M}_v(\mathbf{u}) = \{(\nabla \times \mathbf{u})(v_i), i = 1, 2, \dots, 4\}.$$

- Edge DOFs $\mathbf{M}_e(\mathbf{u})$ at all the edges e_i of K (with the unit tangential vector $\boldsymbol{\tau}_i$):

$$\begin{aligned} \mathbf{M}_e(\mathbf{u}) &= \left\{ \int_{e_i} \mathbf{u} \cdot \boldsymbol{\tau}_i q ds \mid q \in P_{k-2}(e_i), i = 1, 2, \dots, 4 \right\} \\ &\cup \left\{ \int_{e_i} \nabla \times \mathbf{u} q ds \mid q \in P_{k-3}(e_i), i = 1, 2, \dots, 4 \right\}. \end{aligned}$$

- Interior DOFs $\mathbf{M}_K(\mathbf{u})$:

$$\mathbf{M}_K(\mathbf{u}) = \left\{ \int_K \mathbf{u} \cdot \mathbf{q} dA \mid \mathbf{q} \in \mathcal{G}_1 \oplus \mathcal{G}_2 \right\},$$

where $\mathcal{G}_1 = \{\mathbf{q} \mid \mathbf{q} = \psi \mathbf{x} \forall \psi \in Q_{k-3}(K)\}$ and $\mathcal{G}_2 = \{\mathbf{q} \mid \mathbf{q} = \nabla \times \varphi \forall \varphi \in Q_{k-3}(K)/\mathbb{R}\}$ when $k \geq 3$; $\mathcal{G}_1 = \mathcal{G}_2 = \emptyset$ when $k = 2$.

The same theoretical results as those for the triangular elements can be obtained by a similar argument.

5. Two families of curl-curl-conforming elements with $r = k$ and $r = k + 1$. The curl-curl-conforming elements introduced in [22, 23] are restricted to high-order cases, i.e., $k \geq 4$ for triangular elements and $k \geq 3$ for rectangular elements in [23], and $k \geq 4$ for triangular elements in [22]. Rectangular elements are missing in [22].

In this section, we will construct two families of curl-curl-conforming elements by setting $r = k$ and $r = k + 1$ with $k \geq 2$. The two families of elements contain the elements in [22, 23]. Properties similar to those in [22, 23] hold for the generalizations below. For brevity, we only present the definitions and the approximation properties of the V_h spaces.

5.1. A family of curl-curl-conforming elements with $r = k$. By taking $r = k$, we obtain another family of finite element complexes, i.e.,

$$(5.1) \quad 0 \longrightarrow \mathbb{R} \xrightarrow{\subset} \Sigma_h^k \xrightarrow{\nabla} V_h^{k-1,k} \xrightarrow{\nabla \times} W_h^{k-1} \longrightarrow 0.$$

Recall that Σ_h^k is the Lagrange finite element space of order k , and $V_h^{k-1,k}(K) = \nabla P_k(K) \oplus \mathfrak{p}W_h(K)$ or $V_h^{k-1,k}(K) = \nabla Q_k(K) \oplus \mathfrak{p}W_h(K)$ with $k \geq 2$. By Lemma 3.4, $V_h^{k-1,k}(K)$ contains $\mathbf{P}_{k-1}(K)$. More precisely,

$$\begin{aligned} V_h^{k-1,k}(K) &= \mathcal{R}_k \triangleq \mathbf{P}_{k-1} \oplus \{\mathbf{u} \in \tilde{\mathbf{P}}_k \mid \mathbf{u} \cdot \mathbf{x} = 0\} \text{ when } k \geq 4 \text{ and } K \text{ is a triangle,} \\ V_h^{k-1,k}(K) &= Q_{k-1,k} \times Q_{k,k-1} \text{ when } k \geq 3 \text{ and } K \text{ is a rectangle,} \end{aligned}$$

which can be proved by an argument similar to the proof of Lemma 3.4.

For the triangular elements with $k \geq 4$ (rectangular elements with $k \geq 3$), $V_h^{k-1,k}$ coincides with the curl-curl-conforming elements in [23]. Here we extend these finite elements to lower order by allowing $k = 2$ or 3. The sequence of the lowest-order case is shown in Figure 2. These elements have nine DOFs on a triangle and 13 DOFs on a rectangle.

5.1.1. Triangular elements. We define the following DOFs for $V_h^{k-1,k}(K) = \nabla P_k(K) \oplus \mathfrak{p}W_h^{k-1}(K)$:

- Vertex DOFs $\mathbf{M}_v(\mathbf{u})$ at all the vertices v_i of K :

$$\mathbf{M}_v(\mathbf{u}) = \{(\nabla \times \mathbf{u})(v_i), i = 1, 2, 3\}.$$

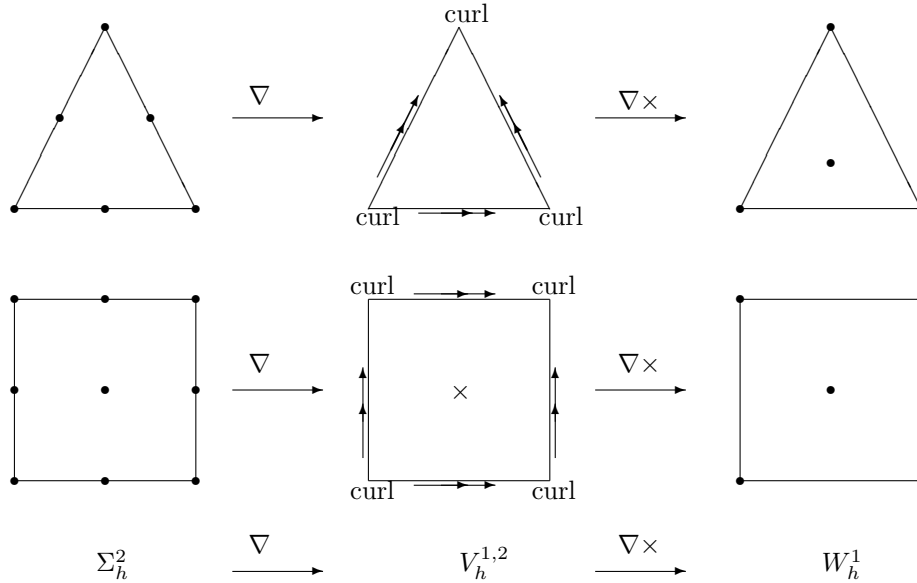
- Edge DOFs $\mathbf{M}_e(\mathbf{u})$ at all the edges e_i of K (with the unit tangential vector τ_i):

$$\begin{aligned} \mathbf{M}_e(\mathbf{u}) &= \left\{ \int_{e_i} \mathbf{u} \cdot \tau_i q \, ds \mid q \in P_{k-1}(e_i), i = 1, 2, 3 \right\} \\ &\cup \left\{ \int_{e_i} \nabla \times \mathbf{u} q \, ds \mid q \in P_{k-3}(e_i), i = 1, 2, 3 \right\}. \end{aligned}$$

- Interior DOFs $\mathbf{M}_K(\mathbf{u})$:

$$\mathbf{M}_K(\mathbf{u}) = \left\{ \int_K \mathbf{u} \cdot \mathbf{q} \, dA \mid \mathbf{q} \in \mathcal{D} \right\},$$

where $\mathcal{D} = \mathbf{P}_{k-5}(K) \oplus \tilde{\mathbf{P}}_{k-5}\mathbf{x} \oplus \tilde{\mathbf{P}}_{k-4}\mathbf{x} \oplus \tilde{\mathbf{P}}_{k-3}\mathbf{x}$ when $k \geq 5$, $\mathcal{D} = \mathbf{P}_{k-3}\mathbf{x}$ when $k = 3, 4$, and $\mathcal{D} = \emptyset$ when $k = 2$.

FIG. 2. The lowest-order ($k = 2$) finite element complex (5.1) in 2D.

5.1.2. Rectangular elements. Similarly, we can extend the rectangular elements to the case of $k = 2$. The DOFs for $\mathbf{u} \in V_h^{k-1,k}(K) = \nabla Q_k(K) \oplus \mathfrak{p}W_h^{k-1}(K)$ are given by the following:

- Vertex DOFs $\mathbf{M}_v(\mathbf{u})$ at all the vertices v_i of K :

$$\mathbf{M}_v(\mathbf{u}) = \{(\nabla \times \mathbf{u})(v_i), i = 1, 2, \dots, 4\}.$$

- Edge DOFs $\mathbf{M}_e(\mathbf{u})$ at all the edges e_i of K , each with the unit tangential vector τ_i :

$$\begin{aligned} \mathbf{M}_e(\mathbf{u}) &= \left\{ \int_{e_i} \mathbf{u} \cdot \tau_i q ds \mid q \in P_{k-1}(e_i), i = 1, 2, \dots, 4 \right\} \\ &\cup \left\{ \int_{e_i} \nabla \times \mathbf{u} q ds \mid q \in P_{k-3}(e_i) \mid i = 1, 2, \dots, 4 \right\}. \end{aligned}$$

- Interior DOFs $\mathbf{M}_K(\mathbf{u})$:

$$\mathbf{M}_K(\mathbf{u}) = \left\{ \int_K \mathbf{u} \cdot \mathbf{q} dA \mid \mathbf{q} \in \mathcal{G}_1 \oplus \mathcal{G}_2 \right\},$$

where $\mathcal{G}_1 = \{\mathbf{q} \mid \mathbf{q} = \psi \mathbf{x} \forall \psi \in Q_{k-2}(K)\}$ and $\mathcal{G}_2 = \{\mathbf{q} \mid \mathbf{q} = \nabla \times \varphi \forall \varphi \in Q_{k-3}(K)/\mathbb{R}\}$ when $k \geq 3$; $\mathcal{G}_1 = \{\mathbf{x}\}$ and $\mathcal{G}_2 = \emptyset$ when $k = 2$.

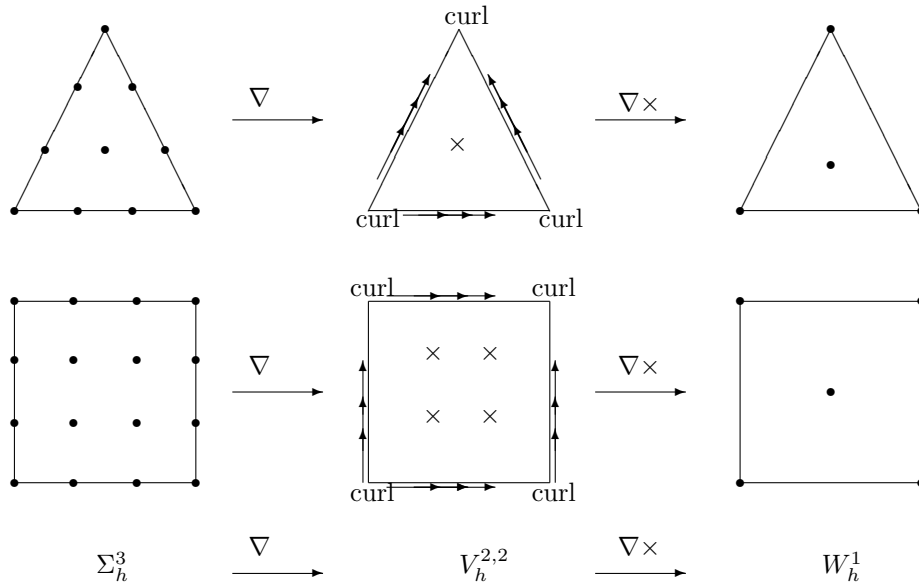
THEOREM 5.1. If $\mathbf{u} \in \mathbf{H}^s(\Omega)$ and $\nabla \times \mathbf{u} \in H^s(\Omega)$, $1 + \delta \leq s \leq k$ with $\delta > 0$, then we have the following error estimates for the interpolation Π_h :

$$(5.2) \quad \|\mathbf{u} - \Pi_h \mathbf{u}\| \leq Ch^s (\|\mathbf{u}\|_s + \|\nabla \times \mathbf{u}\|_s),$$

$$(5.3) \quad \|\nabla \times (\mathbf{u} - \Pi_h \mathbf{u})\| \leq Ch^s \|\nabla \times \mathbf{u}\|_s,$$

$$(5.4) \quad \|(\nabla \times)^2 (\mathbf{u} - \Pi_h \mathbf{u})\| \leq Ch^{s-1} \|\nabla \times \mathbf{u}\|_s.$$

Proof. From Lemma 3.4, $\mathbf{P}_{k-1}(K) \subseteq V_h^{k-1,k}(K)$ and $\mathbf{P}_{k-1}(K) \subseteq W_h^{k-1}(K)$. \square

FIG. 3. The lowest-order ($k = 2$) finite element complex (5.5) in 2D.

5.2. A family of curl-curl-conforming elements with $r = k + 1$. We take $r = k + 1$ in (3.1) for $k \geq 2$ to get the following complex:

$$(5.5) \quad 0 \longrightarrow \mathbb{R} \xrightarrow{\subset} \Sigma_h^{k+1} \xrightarrow{\nabla} V_h^{k,k} \xrightarrow{\nabla \times} W_h^{k-1} \longrightarrow 0.$$

We note that $V_h^{k,k}(K) = \mathbf{P}_k(K)$ when $k \geq 4$ and K is a triangle, and thus $V_h^{k,k}(K)$ on triangles coincides with the finite elements constructed in [22] for $k \geq 4$. The lower-order triangular elements and the entire family of rectangular elements fill the gap in [22].

The lowest-order cases are shown in Figure 3. The number of DOFs of the lowest-order element is 13 for a triangle and 20 for a rectangle.

5.2.1. Triangular elements. The DOFs for $\mathbf{u} \in V_h^{k,k}(K) = \nabla P_{k+1}(K) \oplus \mathbf{p} W_h^{k-1}(K)$ are given as follows:

- Vertex DOFs $\mathbf{M}_v(\mathbf{u})$ at all the vertices v_i of K :

$$\mathbf{M}_v(\mathbf{u}) = \{(\nabla \times \mathbf{u})(v_i), i = 1, 2, 3\}.$$

- Edge DOFs $\mathbf{M}_e(\mathbf{u})$ at all the edges e_i of K , each with the unit tangential vector $\boldsymbol{\tau}_i$:

$$\begin{aligned} \mathbf{M}_e(\mathbf{u}) &= \left\{ \int_{e_i} \mathbf{u} \cdot \boldsymbol{\tau}_i q \, ds \mid q \in P_k(e_i), i = 1, 2, 3 \right\} \\ &\cup \left\{ \int_{e_i} \nabla \times \mathbf{u} q \, ds \mid q \in P_{k-3}(e_i), i = 1, 2, 3 \right\}. \end{aligned}$$

- Interior DOFs $\mathbf{M}_K(\mathbf{u})$:

$$\mathbf{M}_K(\mathbf{u}) = \left\{ \int_K \mathbf{u} \cdot \mathbf{q} \, dA \mid \mathbf{q} \in \mathcal{D} \right\},$$

where $\mathcal{D} = \mathbf{P}_{k-5}(K) \oplus \tilde{\mathbf{P}}_{k-5}\mathbf{x} \oplus \tilde{\mathbf{P}}_{k-4}\mathbf{x} \oplus \tilde{\mathbf{P}}_{k-3}\mathbf{x} \oplus \tilde{\mathbf{P}}_{k-2}\mathbf{x}$ when $k \geq 5$; $\mathcal{D} = \mathbf{P}_{k-2}\mathbf{x}$ when $k = 2, 3, 4$.

5.2.2. Rectangular elements. We extend the construction in [22] to the rectangular case. The DOFs for $\mathbf{u} \in V_h^{k,k}(K) = \nabla Q_{k+1}(K) \oplus \mathbf{p}W_h^{k-1}(K)$ are given by the following:

- Vertex DOFs $\mathbf{M}_v(\mathbf{u})$ at all the vertices v_i of K :

$$\mathbf{M}_v(\mathbf{u}) = \{(\nabla \times \mathbf{u})(v_i), i = 1, 2, \dots, 4\}.$$

- Edge DOFs $\mathbf{M}_e(\mathbf{u})$ at all the edges e_i of K , each with the unit tangential vector τ_i :

$$\begin{aligned} \mathbf{M}_e(\mathbf{u}) &= \left\{ \int_{e_i} \mathbf{u} \cdot \tau_i q \, ds \mid q \in P_k(e_i), i = 1, 2, \dots, 4 \right\} \\ &\cup \left\{ \int_{e_i} \nabla \times \mathbf{u} q \, ds \mid q \in P_{k-3}(e_i), i = 1, 2, \dots, 4 \right\}. \end{aligned}$$

- Interior DOFs $\mathbf{M}_K(\mathbf{u})$:

$$\mathbf{M}_K(\mathbf{u}) = \left\{ \int_K \mathbf{u} \cdot \mathbf{q} \, dA \mid \mathbf{q} \in \mathcal{G}_1 \oplus \mathcal{G}_2 \right\},$$

where $\mathcal{G}_1 = \{\mathbf{q} \mid \mathbf{q} = \psi \mathbf{x} \forall \psi \in Q_{k-1}(K)\}$ and $\mathcal{G}_2 = \{\mathbf{q} \mid \mathbf{q} = \nabla \times \varphi \forall \varphi \in Q_{k-3}(K)/\mathbb{R}\}$ when $k \geq 3$; $\mathcal{G}_2 = \emptyset$ when $k = 2$.

This family of elements leads to one-order-higher accuracy in L^2 -norms.

THEOREM 5.2. *If $\mathbf{u} \in \mathbf{H}^{s+1}(\Omega)$, $1 + \delta \leq s \leq k$ with $\delta > 0$, then we have the following error estimates for the interpolation Π_h :*

$$(5.6) \quad \|\mathbf{u} - \Pi_h \mathbf{u}\| \leq Ch^{s+1} \|\mathbf{u}\|_{s+1},$$

$$(5.7) \quad \|\nabla \times (\mathbf{u} - \Pi_h \mathbf{u})\| \leq Ch^s \|\mathbf{u}\|_{s+1},$$

$$(5.8) \quad \|(\nabla \times)^2 (\mathbf{u} - \Pi_h \mathbf{u})\| \leq Ch^{s-1} \|\mathbf{u}\|_{s+1}.$$

Proof. From Lemma 3.4, $\mathbf{P}_k(K) \subseteq V_h^{k,k}(K)$ and $\mathbf{P}_{k-1}(K) \subseteq W_h^{k-1}(K)$. \square

Remark 5.3. By the duality argument, in the sense of the L^2 -norm, the numerical solution \mathbf{u}_h converges to the exact solution \mathbf{u} with an order of $\min\{s+1, 2(s-1)\}$. Hence, when $s < 3$ the convergence order is $2(s-1)$.

6. Numerical experiments. In this section, we use the three families of the $H(\text{curl}^2)$ -conforming finite elements to solve the quad-curl problem.

For $\mathbf{f} \in H(\text{div}^0; \Omega)$, find \mathbf{u} , such that

$$\begin{aligned} (6.1) \quad &(\nabla \times)^4 \mathbf{u} + \mathbf{u} = \mathbf{f} \quad \text{in } \Omega, \\ &\nabla \cdot \mathbf{u} = 0 \quad \text{in } \Omega, \\ &\mathbf{u} \times \mathbf{n} = 0 \quad \text{on } \partial\Omega, \\ &\nabla \times \mathbf{u} = 0 \quad \text{on } \partial\Omega. \end{aligned}$$

Here $H(\text{div}^0; \Omega)$ is the space of $\mathbf{L}^2(\Omega)$ functions with vanishing divergence, i.e.,

$$H(\text{div}^0; \Omega) := \{\mathbf{u} \in \mathbf{L}^2(\Omega) : \nabla \cdot \mathbf{u} = 0\},$$

and \mathbf{n} is the unit outward normal vector to $\partial\Omega$. Taking divergence on both sides of the first equation of (6.1), we see that the divergence-free condition $\nabla \cdot \mathbf{u} = 0$ holds automatically.

We define $H_0(\text{curl}^2; \Omega)$ with vanishing boundary conditions as

$$H_0(\text{curl}^2; \Omega) := \{\mathbf{u} \in H(\text{curl}^2; \Omega) : \mathbf{n} \times \mathbf{u} = 0 \text{ and } \nabla \times \mathbf{u} = 0 \text{ on } \partial\Omega\}.$$

The variational formulation reads as follows: find $\mathbf{u} \in H_0(\text{curl}^2; \Omega)$, such that

$$(6.2) \quad a(\mathbf{u}, \mathbf{v}) = (\mathbf{f}, \mathbf{v}) \quad \forall \mathbf{v} \in H_0(\text{curl}^2; \Omega),$$

with $a(\mathbf{u}, \mathbf{v}) := (\nabla \times \nabla \times \mathbf{u}, \nabla \times \nabla \times \mathbf{v}) + (\mathbf{u}, \mathbf{v})$.

We define the finite element space with vanishing boundary conditions as

$$V_h^0 = \{\mathbf{v}_h \in V_h^{r-1,k} : \mathbf{n} \times \mathbf{v}_h = 0 \text{ and } \nabla \times \mathbf{v}_h = 0 \text{ on } \partial\Omega\}.$$

Remark 6.1. To enforce the vanishing boundary conditions, we need only set all the DOFs on $\partial\Omega$ to 0.

The $H(\text{curl}^2)$ -conforming finite element method reads as follows: seek $\mathbf{u}_h \in V_h^0$, such that

$$(6.3) \quad a(\mathbf{u}_h, \mathbf{v}_h) = (\mathbf{f}, \mathbf{v}_h) \quad \forall \mathbf{v}_h \in V_h^0.$$

We now turn to a concrete example. We consider the problem (6.1) on a unit square $\Omega = (0, 1) \times (0, 1)$ with an exact solution

$$(6.4) \quad \mathbf{u} = \begin{pmatrix} 3\pi \sin^3(\pi x) \sin^2(\pi y) \cos(\pi y) \\ -3\pi \sin^3(\pi y) \sin^2(\pi x) \cos(\pi x) \end{pmatrix}.$$

Then the source term \mathbf{f} can be obtained by a simple calculation.

The finite element solution is denoted by \mathbf{u}_h . To measure the error between the exact solution and the finite element solution, we denote

$$\mathbf{e}_h = \mathbf{u} - \mathbf{u}_h.$$

6.1. The new family of elements with $r = k - 1$. We first use the lowest-order element in the new family with $r = k - 1$ to solve the problem (6.1). In this test, we use uniform triangular meshes and uniform rectangular meshes, with the mesh size h varying from 1/20 to 1/320 by the bisection strategy. For $\mathbf{u} = (u_1, u_2)^T$, we define two discrete norms,

$$(6.5) \quad \|\mathbf{u}\|_V^2 = \sum_{K \in \mathcal{T}_h} 2h_x^K \int_{y_c^K - h_y^K}^{y_c^K + h_y^K} u_1^2(x_c^K, y) dy + \sum_{K \in \mathcal{T}_h} 2h_y^K \int_{x_c^K - h_x^K}^{x_c^K + h_x^K} u_2^2(x, y_c^K) dx,$$

$$(6.6) \quad \|\mathbf{u}\|_W^2 = \sum_{K \in \mathcal{T}_h} 4h_x^K h_y^K [u_1^2(x_c^K, y_c^K) + u_2^2(x_c^K, y_c^K)],$$

where $K = (x_c^K - h_x^K, x_c^K + h_x^K) \times (y_c^K - h_y^K, y_c^K + h_y^K)$ and $x_c^K, y_c^K, h_x^K, h_y^K$ are as defined in Figure 4.

Table 1 illustrates various errors and convergence rates for triangular elements. Table 2 shows errors measured in various norms for rectangular elements. We also depict error curves for rectangular elements with a log-log scale in Figure 5. We

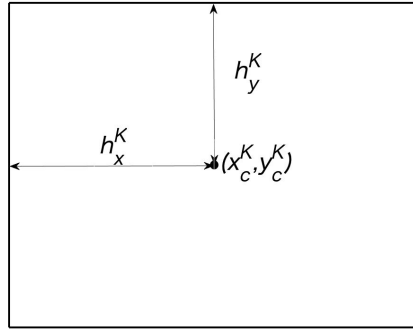


FIG. 4. A rectangular element.

TABLE 1

Numerical results by the lowest-order ($k = 2$) triangular element in the new family ($r = k - 1$) of $H(\text{curl}^2)$ -conforming elements.

h	$\ \mathbf{e}_h\ $	Rates	$\ \nabla \times \mathbf{e}_h\ $	Rates	$\ (\nabla \times)^2 \mathbf{e}_h\ $	Rates
1/20	2.099367e-01		7.598390e-01		2.510488e+01	
1/40	9.736039e-02	1.1085	1.960868e-01	1.9542	1.258823e+01	0.9959
1/80	4.759381e-02	1.0326	4.941757e-02	1.9884	6.297909e+00	0.9991
1/160	2.365626e-02	1.0086	1.237934e-02	1.9971	3.149406e+00	0.9998
1/320	1.183872e-02	0.9987	3.096531e-03	1.9992	1.574759e+00	0.9999

TABLE 2

Numerical results by the lowest-order ($k = 2$) rectangular element in the new family ($r = k - 1$) of $H(\text{curl}^2)$ -conforming elements.

h	$\ \mathbf{e}_h\ $	$\ \mathbf{e}_h\ _V$	$\ \nabla \times \mathbf{e}_h\ $	$\ (\nabla \times)^2 \mathbf{e}_h\ $	$\ (\nabla \times)^2 \mathbf{e}_h\ _W$
1/20	1.56953e-01	3.83651e-02	2.63065e-01	1.48431e+01	3.23332e+00
1/40	5.76799e-02	9.62913e-03	6.58847e-02	7.41177e+00	8.08779e-01
1/80	2.84156e-02	2.40963e-03	1.64788e-02	3.70484e+00	2.02224e-01
1/160	1.41756e-02	6.02611e-04	4.12019e-03	1.85230e+00	5.05578e-02
1/320	7.08507e-03	2.08784e-04	1.03009e-03	9.26132e-01	1.26397e-02

observe that the numerical solution converges to the exact solution with a convergence order of one in the L^2 -norm, two in the $H(\text{curl})$ -norm, and one in the $H(\text{curl}^2)$ -norm, respectively. From Figure 5, we also observe some superconvergence phenomena of \mathbf{e}_h and $(\nabla \times)^2 \mathbf{e}_h$ measured in the sense of (6.5) and (6.6), respectively. Using these superconvergent results, together with some recovery techniques, we can construct a solution with higher accuracy if needed.

6.2. The family of elements with $r = k$. We now use the lowest-order element $V_h^{k-1,k}$ in the family with $r = k$.

Again, we use the uniform mesh. Tables 3 and 4 demonstrate the numerical results with h varying from 1/10 to 1/160. We observe a second-order convergence in the L^2 -norm and $H(\text{curl})$ -norm, and a first-order convergence in the $H(\text{curl}^2)$ -norm.

6.3. The family of elements with $r = k + 1$. We now test elements in the family with $r = k + 1$. We apply the same mesh as before. Tables 5, 6, and 7 show the numerical results for various mesh sizes and elements. We observe the same convergence behavior as in Theorem 5.2.

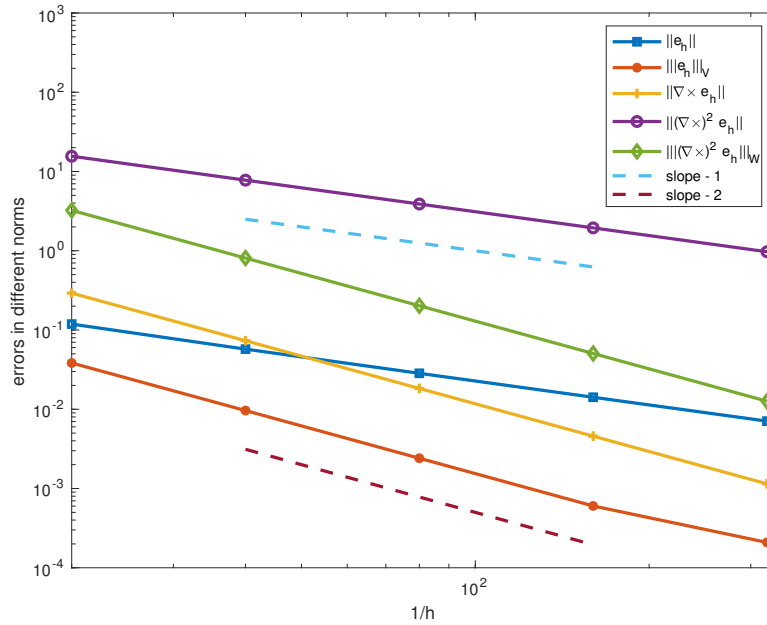


FIG. 5. Error curves in different norms.

TABLE 3

Numerical results by the lowest-order ($k = 2$) triangular element in the family of $H(\text{curl}^2)$ -conforming elements with $r = k$.

h	$\ e_h\ $	Rates	$\ \nabla \times e_h\ $	Rates	$\ (\nabla \times)^2 e_h\ $	Rates
1/10	1.924001e-01		1.836748e+00		4.822043e+01	
1/20	5.037761e-02	1.9333	4.924701e-01	1.8990	2.491412e+01	0.9527
1/40	1.275089e-02	1.9822	1.253756e-01	1.9738	1.256258e+01	0.9878
1/80	3.197749e-03	1.9955	3.148802e-02	1.9934	6.294644e+00	0.9969
1/160	8.016954e-04	1.9959	7.881059e-03	1.9983	3.148996e+00	0.9992

TABLE 4

Numerical results by the lowest-order ($k = 2$) rectangular element in the family of $H(\text{curl}^2)$ -conforming elements with $r = k$.

h	$\ e_h\ $	Rates	$\ \nabla \times e_h\ $	Rates	$\ (\nabla \times)^2 e_h\ $	Rates
1/10	8.545193e-02		7.742300e-01		3.116513e+01	
1/20	2.117547e-02	2.0127	1.924503e-01	2.0083	1.556844e+01	1.0013
1/40	5.283250e-03	2.0029	4.804726e-02	2.0020	7.782876e+00	1.0002
1/80	1.320165e-03	2.0007	1.200780e-02	2.0005	3.891283e+00	1.0001
1/160	3.301818e-04	1.9994	3.001698e-03	2.0001	1.945622e+00	1.0000

We conclude this section by pointing out that the three families of elements bear their own advantages. The new family ($r = k - 1$) can be the best choice if we pursue a low computational cost, while the family with $r = k + 1$ stands out for its higher accuracy in the L^2 -norm.

7. Conclusion. In this paper, we constructed finite element de Rham complexes with enhanced smoothness in 2D. The new construction yields several curl-curl-

TABLE 5

Numerical results by the lowest-order ($k = 2$) triangular element in the family of $H(\text{curl}^2)$ -conforming elements with $r = k + 1$.

h	$\ \mathbf{e}_h\ $	Rates	$\ \nabla \times \mathbf{e}_h\ $	Rates	$\ (\nabla \times)^2 \mathbf{e}_h\ $	Rates
1/10	1.916204e-01		1.831377e+00		4.821773e+01	
1/20	4.953536e-02	1.9517	4.921121e-01	1.8959	2.491403e+01	0.9526
1/40	1.254233e-02	1.9817	1.253529e-01	1.9730	1.256258e+01	0.9878
1/80	3.145763e-03	1.9953	3.148659e-02	1.9932	6.294644e+00	0.9969
1/160	7.897003e-04	1.9940	7.880958e-03	1.9983	3.148996e+00	0.9992

TABLE 6

Numerical results by the lowest-order ($k = 2$) rectangular element in the family of $H(\text{curl}^2)$ -conforming elements with $r = k + 1$.

h	$\ \mathbf{e}_h\ $	Rates	$\ \nabla \times \mathbf{e}_h\ $	Rates	$\ (\nabla \times)^2 \mathbf{e}_h\ $	Rates
1/10	8.399241e-02		7.736407e-01		3.117602e+01	
1/20	2.055671e-02	2.0306	1.924122e-01	2.0075	1.556987e+01	1.0017
1/40	5.125523e-03	2.0038	4.804486e-02	2.0017	7.783057e+00	1.0003
1/80	1.280556e-03	2.0009	1.200764e-02	2.0004	3.891305e+00	1.0001
1/160	3.203172e-04	1.9992	3.001689e-03	2.0001	1.945625e+00	1.0000

TABLE 7

Numerical results by the third-order ($k = 3$) rectangular element in the family of $H(\text{curl}^2)$ -conforming elements with $r = k + 1$.

h	$\ \mathbf{e}_h\ $	Rates	$\ \nabla \times \mathbf{e}_h\ $	Rates	$\ (\nabla \times)^2 \mathbf{e}_h\ $	Rates
1/4	6.482470e-02		9.955505e-01		2.796216e+01	
1/8	4.580398e-03	3.8230	1.388809e-01	2.8416	7.337119e+00	1.9302
1/16	2.927226e-04	3.9679	1.780427e-02	2.9636	1.854476e+00	1.9842
1/32	1.838464e-05	3.9930	2.239038e-03	2.9913	4.648552e-01	1.9962
1/64	1.166284e-06	3.9785	2.802981e-04	2.9978	1.162907e-01	1.9990

conforming elements. The two existing families of elements fit into our complexes, and with the idea in this paper, we extend these elements to lower-order cases. The simple elements (e.g., with six DOFs and eight DOFs for the lowest-order cases on triangles and rectangles, respectively) are thus easy to implement.

In the future, we will construct discrete Stokes-type complexes and curl-curl-conforming elements in 3D and further investigate the superconvergence phenomena.

Appendix. The basis functions for the lowest-order element ($r = 1, k = 2$) on the reference rectangle $(-1, 1) \times (-1, 1)$ are listed as follows:

$$\begin{aligned}
 u_1 = & [12x_1^2x_2^3 - 18x_1^2x_2 - 7x_1x_2^2 + 16x_1x_2/3 - 18x_2^3 + 16x_2^2/3 + 20x_2 - 16/3, \\
 & 12x_1^2x_2^3 - 18x_1^2x_2 + x_1x_2^2 - 16x_1x_2/3 - 18x_2^3 + 16x_2^2/3 + 20x_2 - 16/3, \\
 & 12x_1^2x_2^3 - 18x_1^2x_2 + x_1x_2^2 + 16x_1x_2/3 - 18x_2^3 - 16x_2^2/3 + 20x_2 + 16/3, \\
 & 12x_1^2x_2^3 - 18x_1^2x_2 - 7x_1x_2^2 - 16x_1x_2/3 - 18x_2^3 - 16x_2^2/3 + 20x_2 + 16/3, \\
 & - 12x_1^2x_2^3 + 18x_1^2x_2 + 3x_1x_2^2 + 18x_2^3 - 36x_2 + 16, \\
 & 12x_1^2x_2^3 - 18x_1^2x_2 - 3x_1x_2^2 - 18x_2^3 + 36x_2 + 16, \\
 & 12x_1^2x_2^3 - 18x_1^2x_2 - 3x_1x_2^2 - 18x_2^3 + 20x_2, \\
 & 16x_2 + 3x_1x_2^2 - 12x_2x_1^2x_2^2 + 18x_2x_1^2 + 18x_2x_2^2 - 36x_2]/64.
 \end{aligned}$$

$$\begin{aligned}
u_2 = & [3x_1^2x_2^3/16 - 11x_1^2x_2/64 - x_1^2/12 - x_1x_2/12 - 9x_2^3/32 + 9x_2/16 + 1/12, \\
& 3x_1^2x_2^3/16 - 19x_1^2x_2/64 + x_1^2/12 - x_1x_2/12 - 9x_2^3/32 + 9x_2/16 - 1/12, \\
& 3x_1^2x_2^3/16 - 19x_1^2x_2/64 - x_1^2/12 + x_1x_2/12 - 9x_2^3/32 + 9x_2/16 + 1/12, \\
& 3x_1^2x_2^3/16 - 11x_1^2x_2/64 + x_1^2/12 + x_1x_2/12 - 9x_2^3/32 + 9x_2/16 - 1/12, \\
& - 3x_1^2x_2^3/16 + 15x_1^2x_2/64 + 9x_2^3/32 - 9x_2/16, \\
& 3x_1^2x_2^3/16 - 15x_1^2x_2/64 - 9x_2^3/32 + 9x_2/16, \\
& 3x_1^2x_2^3/16 - 15x_1^2x_2/64 - x_1/4 - 9x_2^3/32 + 9x_2/16 + 1/4, \\
& - 3x_1^2x_2^3/16 + 15x_1^2x_2/64 + x_1/4 + 9x_2^3/32 - 9x_2/16 + 1/4].
\end{aligned}$$

The basis functions for the lowest-order element ($r = 1, k = 2$) on the reference triangle are listed as follows:

$$\begin{aligned}
u_1 = & [-4x_1^2x_2^2 - 4x_1x_2^3 + 5x_1x_2^2 + x_1x_2 - x_2/2, \\
& -4x_1^2x_2^2 - 4x_1x_2^3 + 5x_1x_2^2 - (x_1x_2)/3, \\
& -4x_1^2x_2^2 - 4x_1x_2^3 + 5x_1x_2^2 - (2x_1x_2)/3, \\
& 24x_1^2x_2^2 + 24x_1x_2^3 - 30x_1x_2^2, \\
& 24x_1^2x_2^2 + 24x_1x_2^3 - 30x_1x_2^2, \\
& 24x_1^2x_2^2 + 24x_1x_2^3 - 30x_1x_2^2 + 1].
\end{aligned}$$

$$\begin{aligned}
u_2 = & [4x_1^3x_2 + 4x_1^2x_2^2 - 5x_1^2x_2 - x_1x_2 + x_1/2, \\
& 4x_1^3x_2 + 4x_1^2x_2^2 - 5x_1^2x_2 + x_1^2/3, \\
& 4x_1^3x_2 + 4x_1^2x_2^2 - 5x_1^2x_2 - x_1^2/3 + x_1x_2, \\
& -24x_1^3x_2 - 24x_1^2x_2^2 + 30x_1^2x_2, \\
& -24x_1^3x_2 - 24x_1^2x_2^2 + 30x_1^2x_2 - 1, \\
& -24x_1^3x_2 - 24x_1^2x_2^2 + 30x_1^2x_2].
\end{aligned}$$

REFERENCES

- [1] D. N. ARNOLD, *Finite Element Exterior Calculus*, CBMS-NSF Reg. Conf. Ser. Appl. Math. 93, SIAM, 2018, <https://doi.org/10.1137/1.9781611975543>.
- [2] D. N. ARNOLD AND G. AWANOU, *The serendipity family of finite elements*, Found. Comput. Math., 11 (2011), pp. 337–344.
- [3] D. N. ARNOLD, R. FALK, AND R. WINTHER, *Finite element exterior calculus, homological techniques, and applications*, Acta Numer., 15 (2006), pp. 1–155.
- [4] D. N. ARNOLD, R. FALK, AND R. WINTHER, *Finite element exterior calculus: From Hodge theory to numerical stability*, Bull. Amer. Math. Soc., 47 (2010), pp. 281–354.
- [5] D. N. ARNOLD AND A. LOGG, *Periodic table of the finite elements*, SIAM News, 47 (November 2014), p. 1, <https://sinews.siam.org/Details-Page/periodic-table-of-the-finite-elements>.
- [6] S. C. BRENNER, J. CUI, AND L. SUNG, *Multigrid methods based on Hodge decomposition for a quad-curl problem*, Comput. Methods Appl. Math., 19 (2019), pp. 215–232.
- [7] S. C. BRENNER, J. SUN, AND L. SUNG, *Hodge decomposition methods for a quad-curl problem on planar domains*, J. Comput. Sci., 73 (2017), pp. 495–513.
- [8] F. CAKONI AND H. HADDAR, *A variational approach for the solution of the electromagnetic interior transmission problem for anisotropic media*, Inverse Probl. Imaging, 1 (2017), pp. 443–456.
- [9] G. CHEN, W. QIU, AND L. XU, *Analysis of a Mixed Finite Element Method for the quad-curl Problem*, preprint, <https://arxiv.org/abs/1811.06724>, 2018.

- [10] S. H. CHRISTIANSEN, J. HU, AND K. HU, *Nodal finite element de Rham complexes*, Numer. Math., 139 (2018), pp. 411–446.
- [11] S. H. CHRISTIANSEN AND K. HU, *Generalized finite element systems for smooth differential forms and Stokes' problem*, Numer. Math., 140 (2018), pp. 327–371.
- [12] R. S. FALK AND M. NEILAN, *Stokes complexes and the construction of stable finite elements with pointwise mass conservation*, SIAM J. Numer. Anal., 51 (2013), pp. 1308–1326, <https://doi.org/10.1137/120888132>.
- [13] R. HIPTMAIR, *Canonical construction of finite elements*, Math. Comp., 68 (1999), pp. 1325–1346.
- [14] Q. HONG, J. HU, S. SHU, AND J. XU, *A discontinuous Galerkin method for the fourth-order curl problem*, J. Comput. Math., 30 (2012), pp. 565–578.
- [15] P. MONK AND J. SUN, *Finite element methods for Maxwell's transmission eigenvalues*, SIAM J. Sci. Comput., 34 (2012), pp. B247–B264, <https://doi.org/10.1137/110839990>.
- [16] M. NEILAN, *Discrete and conforming smooth de Rham complexes in three dimensions*, Math. Comp., 84 (2015), pp. 2059–2081.
- [17] J. SUN, *Iterative methods for transmission eigenvalues*, SIAM J. Numer. Anal., 49 (2011), pp. 1860–1874, <https://doi.org/10.1137/100785478>.
- [18] J. SUN, *A mixed FEM for the quad-curl eigenvalue problem*, Numer. Math., 132 (2016), pp. 185–200.
- [19] J. SUN, Q. ZHANG, AND Z. ZHANG, *A curl-conforming weak Galerkin method for the quad-curl problem*, BIT, 59 (2019), pp. 1093–1114.
- [20] Z. SUN, J. CUI, F. GAO, AND C. WANG, *Multigrid methods for a quad-curl problem based on C^0 interior penalty method*, Comput. Math. Appl., 76 (2018), pp. 2192–2211.
- [21] C. WANG, Z. SUN, AND J. CUI, *A new error analysis of a mixed finite element method for the quad-curl problem*, Appl. Math. Comput., 349 (2019), pp. 23–38.
- [22] L. WANG, Q. ZHANG, J. SUN, AND Z. ZHANG, *A Priori and A Posterior Error Estimates for the quad-curl Eigenvalue Problem*, preprint, <https://arxiv.org/abs/2007.01330>, 2020.
- [23] Q. ZHANG, L. WANG, AND Z. ZHANG, *$H(\text{curl}^2)$ -conforming finite elements in 2 dimensions and applications to the quad-curl problem*, SIAM J. Sci. Comput., 41 (2019), pp. A1527–A1547, <https://doi.org/10.1137/18M1199988>.
- [24] S. ZHANG, *Mixed schemes for quad-curl equations*, ESAIM Math. Model. Numer. Anal., 52 (2018), pp. 147–161.
- [25] S. ZHANG, *Regular decomposition and a framework of order reduced methods for fourth order problems*, Numer. Math., 138 (2018), pp. 241–271.
- [26] B. ZHENG, Q. HU, AND J. XU, *A nonconforming finite element method for fourth order curl equations in \mathbb{R}^3* , Math. Comp., 80 (2011), pp. 1871–1886.